Structural and Multidisciplinary Optimization (2021) 64:2343–2360
https://doi.org/10.1007/s00158-021-02986-0

RESEARCH PAPER

On a cellular developmental method for layout optimization via the two-point topological derivative

Marcelo H. Kobayashi[1] · Robert A. Canfield[2] · Raymond M. Kolonay[3]

Received: 26 July 2020 / Revised: 15 March 2021 / Accepted: 15 June 2021 / Published online: 14 July 2021

Abstract

This paper introduces a two-point topological derivative for elasticity and a cellular developmental method for layout optimization of structures. The two-point derivative measures the change on a functional due to the addition of a thin ligament between parts of the domain. It contrasts with the existing single-point topological derivatives that measure the change of a functional due to the subtraction of material. Based on the two-point topological derivative, a cellular developmental method is presented, which builds the layout of a structure in a sequence of cellular divisions and cellular dynamics developmental cycles. The methodology introduced in this work can easily account for member sizes and angle constraints among members of the frame, and the optimization can be performed in the free space or in a bounded domain. Benchmark problems are solved to demonstrate the capability of the cellular developmental method to solve optimization problems in structural mechanics.

Keywords Topological derivative · Topology optimization · Structural optimization · Cellular developmental method

1 Introduction

With the advancements in the area of additive manufacturing (AM) the design space for structural concepts has exploded. Additive manufacturing has enabled the use of functionally graded materials, multi-scale structures and endless structural configurations or topologies. In order to take full advantage of all the free design parameters that AM offers, automated design processes must be used.

Structural optimization techniques date back to Michell (1904) who developed techniques to determine the optimal layout of truss structures with stress constraints. Fifty-six years later Schmit (1960) posed the design problem as a non-linear mathematical programming problem in the context of finite elements for the structure, the genesis of modern structural optimization. Structural optimization is typically broken down into the following three areas, based on what the independent design variables are: sizing, shape and topology optimization. For sizing optimization the independent parameters are geometric structural dimensions or cross-sectional properties such as thickness, width, cross-sectional area, moment of inertia or torsional constant. For shape optimization the free design parameters are associated with the boundary of the structure such as joint locations, edges or surfaces. The independent parameters for topology optimization are associated with the presence or absence of structure within the domain of interest. With the addition and subtraction of material, topology optimization, like shape optimization, can move the structure's boundary, but unlike shape optimization it has the freedom to eliminate or create voids within the structure. For this study the primary interest is in topology optimization.

Topology optimization seeks the economical distribution of material in a domain aiming to perform a set of programmable tasks under physical and cost constraints. A comprehensive review of topology optimization techniques can be found in Deaton and Grandhi (2014). Topology

Responsible Editor: Seonho Cho

✉ Marcelo H. Kobayashi
marcelok@hawaii.edu

[1] Department of Mechanical Engineering, University of Hawaii at Manoa, 2540 Dole Street—Holmes Hall 302, Honolulu, HI 96822, USA

[2] Kevin T. Crofton Department of Aerospace and Ocean Engineering, Virginia Polytechnic Institute and State University, Randolph Hall, Rm. 214 460 Old Turner St. (MC 0203), Blacksburg, VA 24061, USA

[3] Air Force Research Laboratory Multidisciplinary Science and Technology Center, 2210 8th Street, Bldg 146, Room 218 WPAFB, OH 45433, USA

optimization can be categorized into two basic classes. Those methods that are based on primitive basic shapes and those based on free-form shapes. The free form methods, such as level set (Allaire et al. 2004) and the Solid Isotropic Material with Penalization (SIMP) (Bendsøe and Sigmund 2003), are very efficient in developing solutions to problems that, at the optimum, have moderate to high volume of material. Methods based on basic shapes, such as cellular based (Kobayashi et al. 2009; Bielefeldt et al. 2019) or geometric projection based (Norato et al. 2015; Smith and Norato 2019), on the other hand, are more efficient in producing optimum solutions that have a low volume of material, since in such cases the shape of each member in the frame is relatively simple and easy to model.

Typical free-form topology optimization methods, such as level set or SIMP, use a gradient-based method for the search of an updated or improved layout. This search is necessarily local in nature, since the gradient on which this search is based conveys relevant information in a neighborhood of its point of calculation only. In topology optimization this local search is particularly limiting, because the landscape of the space where the topology optimization seeks the optimum is partitioned into equivalence classes of objects that can be continuously deformed into each other. In this landscape, the gradient of a functional computed inside one connected component is isolated from the landscape of the design space in other neighboring components. Therefore in a technique such as the level set method, this gradient cannot direct the search to jump from one component to the next where a better solution may be located. As a result, such methods tend to be trapped in a component, as they converge towards a local minimum in the component they started. Density-based methods can generate holes and, therefore, can move between components through these holes. Topology optimization algorithms relying on Hadamard shape derivatives, such as the level set method, cannot predict the change in the objective function at topological changes. Such methods typically rely on a topological derivative, or topological gradient, as it is also known, to create a hole, and thus jump to a different topology that optimizes the reduction of the functional due to the creation of a small hole in the domain. The topological derivative was introduced in the 1990s as the bubble method for topology optimization of structures under compliance constraints (Eschenauer et al. 1994). Later, it was rigorously defined and extended in Sokolowski and Zochowski (1999). After its introduction, the topological derivative has seen exponential growth in both scope and utility within mathematical and engineering forums (see the book (Novotny and Sokolowski 2020), the recent review series (Novotny et al. 2019a, b, c) and the papers cited therein). Despite its diversity in formulation and application, nearly all existing topological derivatives are subtractive in nature. That is, they look for singular sets that identify areas of excess material within the domain. Additive topological-derivatives are few, and the existing ones have not yet been used for topology optimization in the way that subtractive topological derivative has in approaches such level set methods. Indeed, Nazarov et al. (2004, 2005) developed a topological derivative for the energy functional due to the addition of thin ligaments when the state equation is a Poisson equation, Gangl (2020) developed a topological derivative for multi-material problems, and for graphs, such as trusses, Leugering and Sokolowski (2008) performed sensitivity analysis with respect to changing its topology—see also Lee (2008), which considers an asymptotic expansion of the topological gradient for a hole to decide whether an existing hole must be removed or not in the design domain. Recently, an independent work by Dapogny (2020, 2021) considered an additive approach in a different context, where the bar can be a curve in two-dimensional or three-dimensional space. That work uses the material ersatz approximation to replace the linear elasticity system on the frame with an approximate problem on a design domain where the voids in the design domain are filled with a smooth inhomogeneous material that coincides with the frame properties at the frame domain, while extending smoothly to a soft, artificial material at the voids. The two formulations, namely, the formulation proposed in Dapogny (2020, 2021) and the one introduced in this work follow fundamentally different approaches and entail different computations for the calculation of the topological derivatives.

In this paper the additive topological derivative introduced in Nazarov et al. (2004, 2005) is extended to linear elasticity. Furthermore, this topological derivative is used for topology optimization of structures via a novel cellular developmental method. The additive topological derivative seeks to identify suitable pairs of points in the domain that can be connected to improve the performance of the design. To distinguish it from the existing topological derivatives and emphasize the pairing desired, we call the topological derivative of ligaments the two-point topological derivative.

2 Two-point topological derivative

The two-point topological derivative is considered for the compliance functional. Let Ω be a bounded, open set of $\mathbb{R}^N$, $N = 2, 3$, and assume a shape functional $\mathcal{J}$ is given on a convex, working domain D: $\mathbb{R}^N \supset D \supset \Omega$. The two-point topological derivative measures the change in the functional $\mathcal{J}$ due to the addition of a thin ligament connecting two

admissible points at the boundary $\partial\Omega$. The set of admissible pairs, $\mathcal{A}$, is defined as follows:

$$\mathcal{A} = \{(p,q) \in \partial\Omega \times \partial\Omega | \text{ the line } \overline{pq} \text{ lies outside of } \Omega \text{ in a traction-free region}\}.$$

Given an admissible pair of points $(p,q) \in \mathcal{A}$ and a small number $t > 0$, we consider the augmented domain, Ω_t, obtained by adding to Ω a thin ligament, I_t, of thickness t connecting p to q (Fig. 1). The ligament is a thin quadrilateral in the plane or a cylinder in three-dimensional space. If the following limit exists,

$$\mathcal{TJ}(p,q) \stackrel{\text{def}}{=} \lim_{t\downarrow 0} \frac{\mathcal{J}(\Omega + I_t) - \mathcal{J}(\Omega)}{t}, \tag{1}$$

analogously to the definition of the single-point topological derivative (Sokolowski and Zochowski 1999), we call it the **two-point topological derivative** of $\mathcal{J}$ at (p,q). Defining the function $J(t) = \mathcal{J}(\Omega_t)$, for a small parameter $t \geq 0$, we obtain the following asymptotic expansion

$$\mathcal{J}(\Omega_t) = \mathcal{J}(\Omega) + J'(0^+)t + o(t). \tag{2}$$

Linear elasticity Let $\Omega \subset \mathbb{R}^N$, $N = 2, 3$ be a bounded domain in $\mathbb{R}^N$ with a smooth, oriented boundary $\partial\Omega = \Gamma_D \cup \Gamma_N$ filled with a linear, homogeneous, isotropic and elastic material satisfying Hooke's constitutive law. The elasticity tensor is defined by

$$Ae(u) = 2\mu e(u) + \hat{\lambda}\mathrm{Tr}(e(u))I, \tag{3}$$

where I is the $N \times N$ identity matrix,

$$e(u) = \frac{\nabla u + \nabla u^T}{2}, \tag{4}$$

is the small strain tensor, $\hat{\lambda} = \lambda$ for three-dimensional and plane strain problems, $\hat{\lambda} = \lambda(1-2\nu)/(1-\nu)$ for plane stress problems, and λ, μ are the Lamé constants of the material

$$\lambda = \frac{\nu E}{(1+\nu)(1-2\nu)}, \tag{5}$$

$$\mu = \frac{E}{2(1+\nu)}, \tag{6}$$

where ν is the material's Poisson constant and E the material's Young's modulus.

The displacement u in Ω is the solution of the linearized elasticity equation

$$-\nabla.(Ae(u)) = f, \text{ in } \Omega, \tag{7}$$

subject to the following Dirichlet and von Neumann boundary conditions

$$u = 0, \text{ on } \Gamma_D, \tag{8}$$

$$Ae(u).n = g, \text{ on } \Gamma_N, \tag{9}$$

where n is the outward-pointing, unit-normal to $\partial\Omega$ and the superscript ^{T} denotes the transpose of an operator. In the extended domain, $\Omega_t = \Omega + I_t$, the following system is defined

$$-\nabla.(Ae(u)) = f, \text{ in } \Omega_t, \tag{10}$$

$$u_t = 0, \text{ on } \Gamma_D, \tag{11}$$

$$Ae(u_t).n = g, \text{ on } \Gamma_N \setminus \Gamma_t, \tag{12}$$

$$Ae(u_t).n = 0, \text{ on } \Gamma_t, \tag{13}$$

where $\Gamma_t = \partial I_t$ is the boundary of the ligament connecting p to q.

The two-point topological derivative of the compliance functional $\mathcal{J}_c$ between points $p, q \in \mathcal{A}$ and for negligible body forces is given by the following formula (cf. Appendix 1)

$$\mathcal{TJ}_c(p,q) = -\frac{\hat{E}}{|q-p|^3}[(u(q) - u(p)).(q-p)]^2. \tag{14}$$

Note that, since $\hat{E} > 0$, when searching for pairs p, q that provides the smallest value of the two-point, topological derivative $\mathcal{TJ}_c(p,q)$, only the kinematic value of $\frac{\mathcal{TJ}_c(p,q)}{\hat{E}}$ needs to be computed.

3 Cellular developmental method

The layout optimization method introduced in this work is based on a cellular developmental approach for planar frame structures. The frame structure is parameterized over a map, and the developmental process itself is comprised of two stages: a cellular division stage and a cellular dynamics stage.

A **map** is a finite set of regions, where a region is a finite, circular sequence of edges that intersect at vertices. Each edge has two vertices at its boundary and there are no vertices without an incident edge. All edges are part of the boundary of a region and no island can exist within a region (Prusienkiewicz and Lindenmayer 2004). Given a map, a two-step **frame protocol** is used to build the frame layout. In the first step, each edge of the map is thickened according to a thickness parameter assigned to each individual edge.

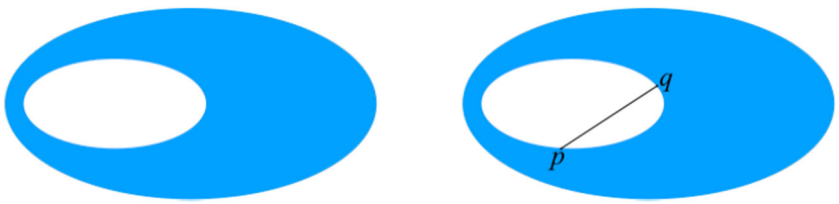

Fig. 1 Domains: unperturbed Ω (left) and perturbed $\Omega_t = \Omega + I_t$ (right). The ligament I_i is a thin quadrilateral or cylinder connecting two admissible points p and q

The result is a set of capped rectangles corresponding to each edge of the map. In the second step, the union of these capped rectangles is effected, thus defining the layout of the frame (Fig. 2). The underlying map of the frame is called the **skeleton**. According to this protocol, the frame layout is defined by a small set of design variables, namely, the pairs of coordinates of each vertex of the skeleton, and the thicknesses of the edges.

With the frame protocol for building the structural frame, the cellular developmental method optimizes the layout through a sequence of cycles, each one comprising a cellular division stage and a cellular dynamics stage. In the **cellular division** stage, the two-point topological derivative is computed at a finite set of sample pairs connecting points along the edges of the skeleton. Then all faces of the skeleton are surveyed, and for each face a line is drawn connecting the pair of selected points with minimum two-point topological derivative, and, therefore, maximal reduction of compliance, among acceptable pairs. In this way, the faces are divided and the frame topology is modified. For simplicity, the two-point topological derivative is computed for samples taken along the edges of the skeleton, and, therefore, at the midline of the edges of the frame.

Figure 3 illustrates the candidate edges and selected edges for the frame depicted in Fig. 2. The load for this illustrative problem corresponds to a downward pointing vertical load applied at vertex 2 of the skeleton. The frame is fixed at vertices 0 and 3, and three points are probed along each edge of the skeleton.

Following the cellular division stage, the **cellular dynamics** stage performs a shape optimization on the new topology of the frame. The introduction of the new edges in the frame causes a disruption in the stress distribution within the frame, which requires an adaption of the shape of the frame for optimal performance. For instance, the new edges added in Fig. 3b cause bending, which induces a transformation of the shape to reduce the bending (see Fig. 5). In this work, the shape optimization is carried out using four mathematical programming algorithms, with compliance as the objective function, subject to area and other constraints such as collision and containment into a domain (cf. Section 4). To compute the sensitivities needed by the shape optimizer, we choose a continuous-discrete approach. This option provides greater flexibility in using existing code, since no access is required to source code that does not provide the discrete sensitivities.

Concretely, the gradient needed for the shape optimizer is computed as follows. Given a general functional

$$\mathcal{J}(\Omega) = \int_{\Omega} j + \int_{\partial\Omega} l, \tag{15}$$

the sensitivity of $\mathcal{J}$ with respect to a shape parameter η, $\partial_\eta \mathcal{J}$, is computed using the chain rule

$$\partial_\eta \mathcal{J} = \mathcal{J}'(\Omega_\eta)(\partial_\eta \Omega_\eta), \tag{16}$$

where Ω_η is the deformed domain obtained by changing the parameter η, $\partial_\eta \Omega_\eta$ is the geometric sensitivity of the shape with respect to the parameter η, and the shape derivative is given by (cf. Allaire 2004)

$$\begin{aligned}\mathcal{J}'(\Omega)(\theta) = &\int_{\Gamma_N} [j(u) + Ae(u) : e(u) - \vartheta.f - \partial_n(g.\vartheta) \\ &- Hg.\vartheta]\theta.n \\ &+ \int_{\Gamma_D} [j(u) - Ae(u) : e(\vartheta)]\theta.n \\ &+ \int_{\partial\Omega} (\partial_n l(u) + Hl(u)), \end{aligned} \tag{17}$$

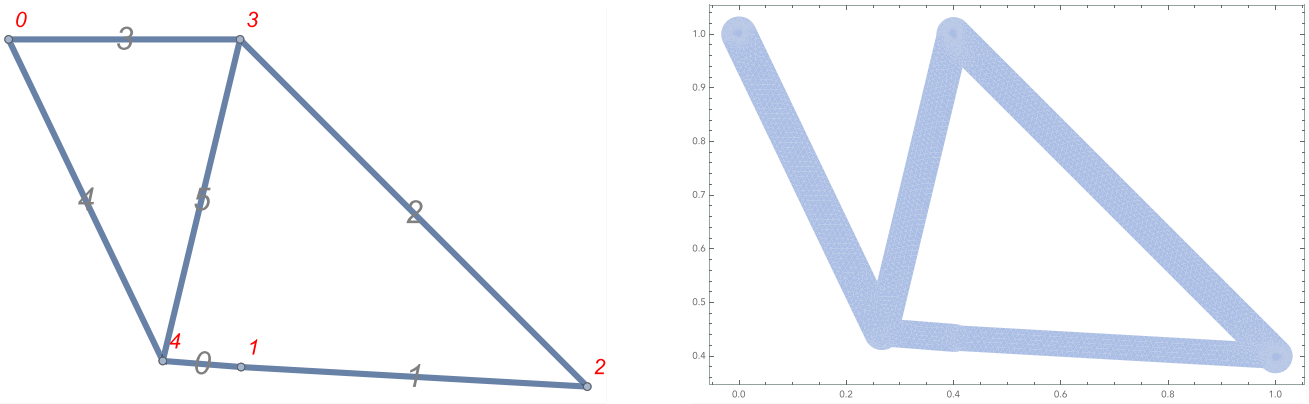

(a) Frame skeleton (b) Frame structure

Fig. 2 Buildup of a frame: (a) the skeleton underlying the frame, with vertices labeled in red and edges labeled in gray; (b) the frame layout resulting from the union of the thickened edges of the skeleton. The edges can have different thicknesses including zero thickness, as is the case of edge *3* of the skeleton

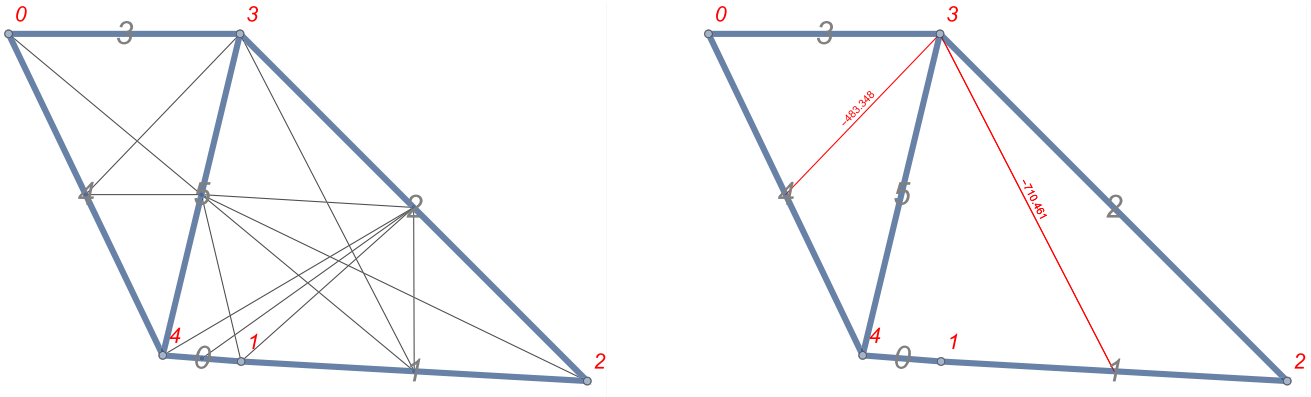

(a) Set of candidate edges (b) Selected edges for cellular division

Fig. 3 Cellular division stage: (a) candidate edges generated by sampling all edges at three points along their extension and applying a constraint on the minimum angle of 15°, (b) selected edges for division, shown in red together with their associated values of $\frac{\mathcal{T}\mathcal{J}_c(p,q)}{\hat{E}}$

$\theta \in W^{1,\infty}(\mathbb{R}^N, \mathbb{R}^N)$. Here the adjoint state, ϑ, satisfies

$$-\nabla.(Ae(\vartheta)) = -j'(u), \text{ in } \Omega \tag{18}$$

$$(Ae(\vartheta).n) = -l'(u), \text{ on } \Gamma_N \tag{19}$$

$$\vartheta = 0, \text{ on } \Gamma_D. \tag{20}$$

For compliance, $j(u) = f.u, l(u) = g.u$ on Γ_N and $l(u) = 0$ on Γ_D and $\vartheta = -u$, since the problem is self-adjoint. Finally, the geometric sensitivity is computed from the parameterization of the thickened edges over the skeleton. Specifically, with the geometry of the capped rectangle defined by five parameters (x_0, y_0, x_1, y_1, h) shown in Fig. 4a, a point at the boundary of the capped rectangle can be identified by the following formulae

$$\mathbf{r}(u) = \mathbf{r_0} + u(\mathbf{r_1} - \mathbf{r_0}) + \frac{sh}{2}\mathbf{n}, \tag{21}$$

for the flat sides, where $\mathbf{r} = (x, y)$, $\mathbf{r_i} = (x_i, y_i)$, $i = 0, 1$, $s = \pm 1$, $\mathbf{n}$ is a unit normal to $\mathbf{r_1} - \mathbf{r_0}$, and $u \in [0, 1]$ is the line parameter; while the half disk around (x_1, y_1) can be parameterized as

$$\mathbf{r}(\theta) = \mathbf{r_1} + \frac{h}{2}\mathbf{R}(\theta)\mathbf{t}, \tag{22}$$

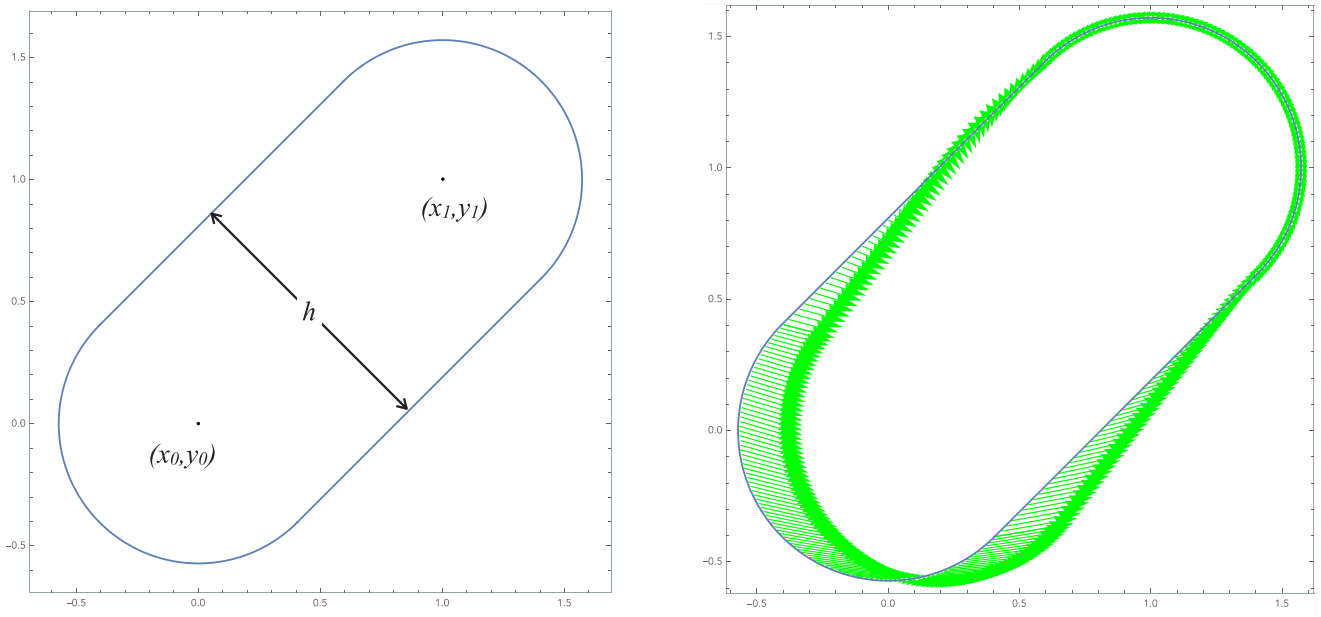

(a) Frame parameterization (b) Geometric sensitivity

Fig. 4 Geometric sensitivities: (a) frame member parameterization; the geometry of a capped rectangle is defined by five parameters: (x_0, y_0, x_1, y_1, h); (b) geometric sensitivity with respect to x_0

where $\mathbf{t}$ is the unit vector along $\mathbf{r_1} - \mathbf{r_0}$, $\mathbf{R}(\theta)$ is the rotation matrix

$$\mathbf{R}(\theta) = \begin{bmatrix} \cos\theta & -\sin\theta \\ \sin\theta & \cos\theta \end{bmatrix}, \tag{23}$$

and $\theta \in [-\pi/2, \pi/2]$ is the line parameter. A similar parameterization is used for the cap around $\mathbf{r_0}$. The geometric sensitivity is then computed by taking the derivative of the parameterized curve with respect to the shape parameters (x_0, y_0, x_1, y_1, h). For instance, the flat sides vary as follows with respect to x_0

$$\partial_{x_0}\mathbf{r} = \left[1 - u - \frac{hs(x_0 - x_1)(y_0 - y_1)}{2\left((x_0 - x_1)^2 + (y_0 - y_1)^2\right)^{3/2}} - \frac{hs(y_0 - y_1)^2}{2\left((x_0 - x_1)^2 + (y_0 - y_1)^2\right)^{3/2}}\right]^T. \tag{24}$$

Figure 4(b) illustrates the computed geometric sensitivity with respect to x_0. The geometric sensitivity for the remaining parts and parameters are computed analogously. After the cellular dynamics stage, the frame in Fig. 3b is transformed into the shape-optimized frame depicted in Fig. 5. The full procedure of the cellular developmental method for layout optimization is summarized in Algorithm 1 below.

Algorithm 1 Cellular developmental method for layout optimization.

Require: functional to be minimized, J, criteria for stopping, criteria for cell division and an initial map

1: **repeat**
2: build the frame using the frame protocol
3: perform shape optimization to compute the position of the vertices and the edge thickness parameters of the map to minimize the functional J
4: **for** each face in the map **do**
5: sample the skeleton edges in the face for admissible pairs
6: compute the two-point topological derivative for all sample pairs
7: compute the set of acceptable pairs, that is, the set of admissible pairs that meet a set of criteria for cellular division
8: select the pair, p, which minimizes the two-point topological derivative among the acceptable pairs
9: divide the face along p
10: **end for**
11: **until** stopping criteria are met

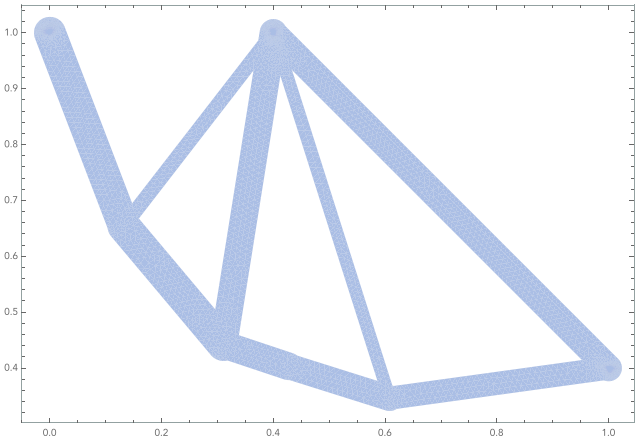

Fig. 5 Frame structure after the shape optimization in the cellular dynamics stage

4 Results and discussion

Compliance minimization for cantilever structures are classic benchmark problems in topology optimization (Bendsøe and Sigmund 2003). Three such benchmarks were studied in this work: a two load-cases, short cantilever problem; a long, single-load cantilever problem, and the L-bracket problem. Besides compliance as the objective function, the area constraint was common to all problems. To compute the sensitivity for the area constraint, the aforementioned continuum-discrete approach to calculate the compliance sensitivity was used again for the computation of the area sensitivity (cf. Allaire et al. 2004)

$$A'(\Omega)\theta = \int_\Omega \theta(x).n(x)ds, \tag{25}$$

where $\theta \in W^{1,\infty}(\mathbb{R}^N, \mathbb{R}^N)$. In addition, a detection and penalization of edge intersection was enforced via the surface-sweep algorithm (de Berg et al. 2010). This algorithm has a complexity of $\mathcal{O}((n + k)\log n)$, where n is the number of edges and k is the number of intersection points induced by these edges. While this last constraint was not strictly necessary, it allows for a logical organization of tasks: the cellular division stage controls the topology of the skeleton, while the cellular dynamics controls the shape and size of the frame.

In all runs, the finite element computations were performed using the open-source library FEniCS (Alnaes et al. 2015), with a cubic Lagrangian element and isoparametric formulation, and the mesh was generated using the open-source library Gmsh (Geuzaine and Remacie 2009). A mesh is generated for each intermediate shape in the computation. In addition, four mathematical programming

algorithms were employed in the computations below: Canfield's implementation of Schittkowski's SQP method (Canfield 2020; Schittkowski 1983), SciPy's (Virtanen et al. 2020) trust region constrained algorithm, and MATLAB's implementation of the active set and interior point methods (MathWorks 2020). These four methods will hereafter be referred to as follows: SQP, TRCA, AS and IP, respectively. Unless mentioned to the contrary, the optimization runs employed a tolerance of 0.001 and a maximum number of iterations of 100 for the first cycles and 500 for the final cycle. In addition, the default options were used with the four methods SQP, TRCA, and IP, except that line search size of 0.1 was used with AS. Sampling of three equally spaced points on each edge of the skeleton were surveyed for cellular division. Finally, all design variables, constraints and objective functions were normalized: the objective function and area constraint values were normalized by a reference value and the target area, respectively, vertex coordinates were normalized by reference lengths and the edge thicknesses were normalized by the minimum and maximum thickness allowed. With the previous normalizations, the normalized parameters range in values $[-1, 1]$. For concreteness, new edges added in each cycle took a normalized thickness of -0.75 or -0.95.

4.1 Short cantilever structure

Realistic structural design invariably involves multiple load cases. As the first test case, we consider the two load-cases, cantilever-problem reported in Andreassen et al. (2011). Here, the clamped support is fixed at two points and the square design domain is imposed on the vertices of the skeleton, rather than the full frame. The material properties for this example were $E = 1$ and $\nu = 0.3$ (note that the optimized topology does not depend on E).

The functional to be minimized in this example is the sum of the compliance for each load-case (Andreassen et al. 2011). Hence, the two-point topological derivative quantifies the reduction of the aggregate compliance of all load-cases. Alternatively, a *minmax* optimization problem could be easily considered, but since the load and supports are symmetric, that would lead to the same solution presented here—generally, however, a *minmax* optimization is preferable since they lead to more robust design. The two load-cases correspond to (i) a unit upward pointing load at the top right and (ii) a unit downward pointing load at the bottom right (Fig. 6).

The initial skeleton was chosen as a minimal graph containing the points of application of loads and the supports, and no optimization of the initial frame was undertaken. Two cellular division cycles were performed and the first and second cycles apply an inequality area constraint: $A \leq 0.4$. A minimal angle of fifteen degrees between the candidate edges and existing edges and a cutoff limit of $\frac{\mathcal{T}\mathcal{J}_c(p,q)}{\hat{E}} < -30$ was also enforced for acceptability of new edges. The latter corresponds to about 1/10,000 of the minimum value in the survey of the candidate pairs after cycle 0.

The layouts, values of compliance and areas for the first cycle obtained by all four optimizers are virtually identical. Therefore only the result for SQP is shown in Fig. 7 as a representative of the results for all four methods. As can be seen from this figure, the optimized layout after the first cycle compares well with that obtained in Andreassen et al. (2011). For reference, the compliance of the optimized solution obtained with SIMP is 68.8 using the code top88.m (Andreassen et al. 2011) with all parameters used in that work, namely, number of elements in x and y directions $n_x = n_y = 150$, volume fraction, $v_f = 0.4$, penalization factor, $p = 3$, filter radius, $r_{min} = 6$, and filtering of the sensitivities; except for the convergence tolerance, here set to 0.001 for consistency with the tolerance set for the cellular developmental method. A direct comparison of the values of the compliance obtained with SIMP and the cellular developmental method is not warranted. Indeed, some material in the cellular division method lays outside of the unit square, which would tend to reduce the compliance for the cellular division method. By contrast, the volume constraint would tend to increase the compliance of the cellular developmental method, since some material lay outside of the domain, and, therefore, the actual volume fraction in the expanded domain is smaller that the volume fraction in SIMP. Finally, the gray material in the SIMP solution requires an interpretation of the optimized solution to determine the true value of the compliance optimized with SIMP. Qualitatively, however, the topology obtained with SIMP and the cellular developmental methods agree well.

The second cycle generated a small reduction in compliance, about 1.5% of the value obtained in the first cycle. For comparison, the reduction of the compliance computed for the initial layout and that computed for the first cycle is 99.1%. The two-point topological derivative provides insight into these different gains. Indeed, in the survey after cycle zero, the minimum value of $\frac{\mathcal{T}\mathcal{J}_c(p,q)}{\hat{E}}$ was -4.53×10^6. After cycle one, the same minimum was now a mere $\frac{\mathcal{T}\mathcal{J}_c(p,q)}{\hat{E}} = -396.13$, or about 0.03% of the minimum after cycle zero. These values of the two-point topological derivative predict a smaller gain for the second cycle when compared to the first cycle. This predictability of the gains after the cellular division makes the two-point topological derivative useful as a criterion for stopping the cellular divisions, as well as to set a cutoff (used here) for $\frac{\mathcal{T}\mathcal{J}_c(p,q)}{\hat{E}}$ of candidate edges.

Despite the small reduction in the compliance, the optimized topologies obtained by the gradient-based methods

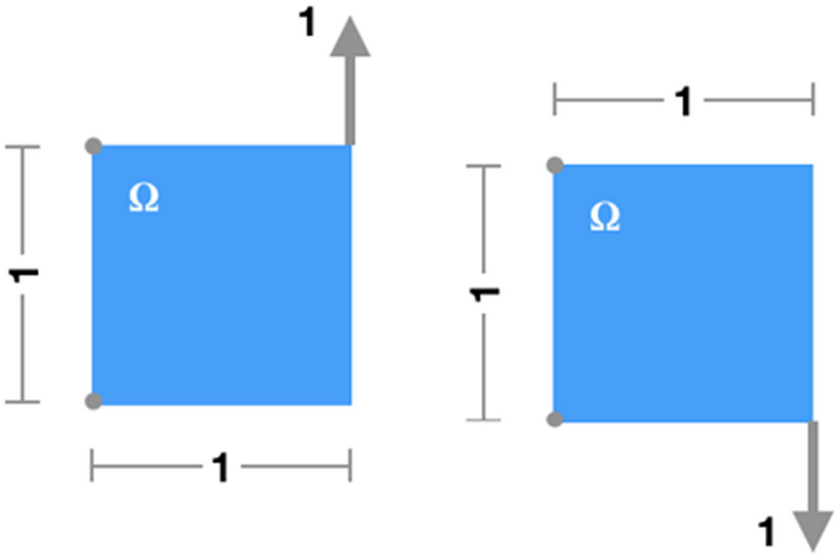

Fig. 6 Design domain for skeleton, external loads and support points (gray disks at left boundary)

are remarkable: SQP and AS developed similar internal substructures and reinforcement of the middle joint, while IP also reinforced the middle joint, but combined the added edges and existing edges to create a tapered shape for the crossing edges. The best performing design, obtained with TRCA, depicts a branched structure with more material closer to the right boundary. The values of compliance of all four methods are close, however, which suggests a flat region in the graph of the objective function around a local optimum (Fig. 8).

Regarding the performance of the four mathematical programming algorithms, Fig. 9 shows the optimization histories of both the compliance convergence and constraint violation for all four methods. At the beginning of each cycle, there is a dip in the compliance and an accompanying increase in the mass and constraint violation due to the addition of the new frame members. The SQP method performed significantly better than the remaining methods, both with respect to the total number of iterations as well as the total number of functions evaluations—note that the number of function evaluations is equal to the number of solutions of the linear system associated with the finite element model of the structure. Compared to SIMP, the cellular developmental method using SQP requires less overall number of iterations or number of function evaluations for convergence, despite the increase in the volume of the frame at the start of each cellular division stage. It is expected that faster convergence of SQP be enhanced with the tightening of the tolerances for convergence, due to its super-linear convergence.

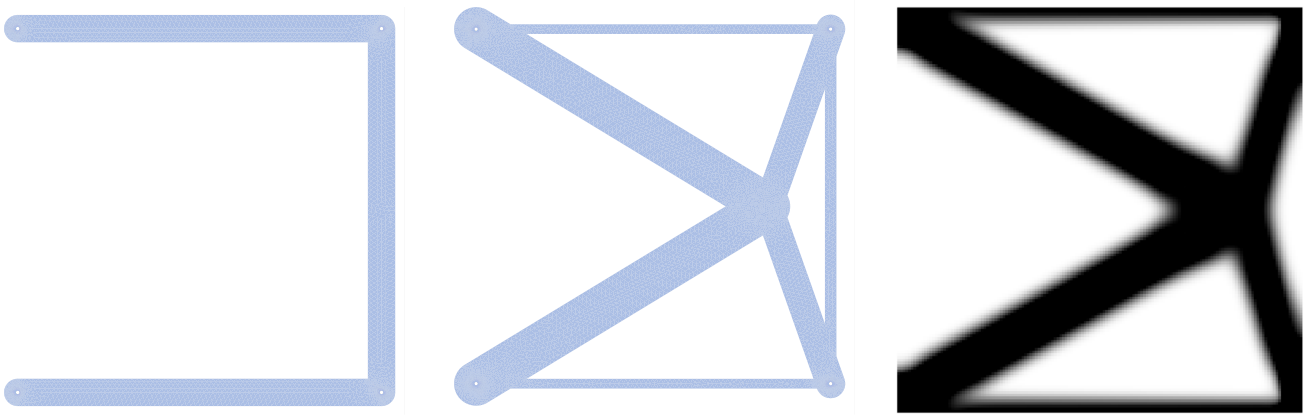

(a) Cycle 0: $\mathcal{J}_c = 5064, A = 0.228$ (b) Cycle 1: $\mathcal{J}_c = 46.8, A = 0.400$ (c) SIMP: $\mathcal{J}_c = 68.8, A = 0.400$

Fig. 7 Short cantilever. (a) Initial layout, (b) optimized layout after the first cycle, (c) optimized solution obtained with SIMP. The target area for this problem is 0.4. The SIMP solution is obtained using the top88.m code listed in Andreassen et al. (2011)

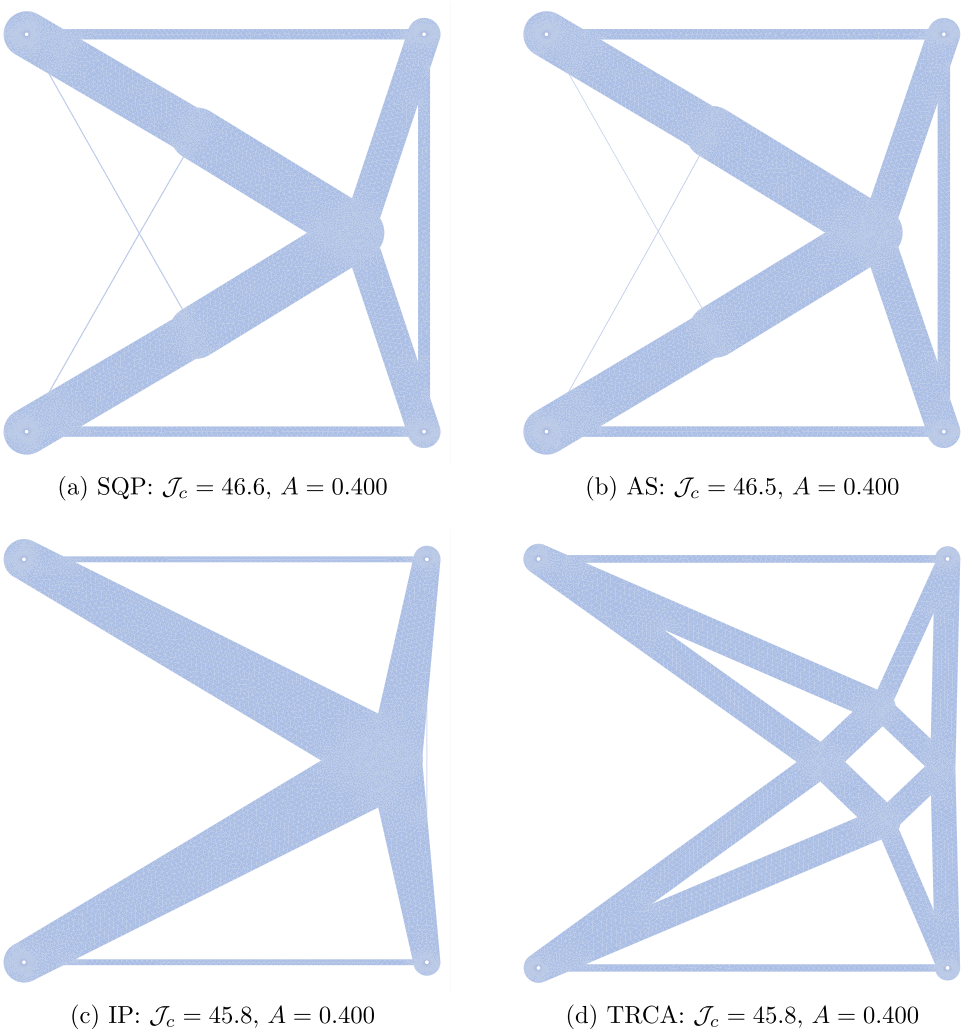

(a) SQP: $\mathcal{J}_c = 46.6,\ A = 0.400$ (b) AS: $\mathcal{J}_c = 46.5,\ A = 0.400$

(c) IP: $\mathcal{J}_c = 45.8,\ A = 0.400$ (d) TRCA: $\mathcal{J}_c = 45.8,\ A = 0.400$

Fig. 8 Short cantilever. Optimized layouts after two cycles obtained with the mathematical programming algorithms SQP, AS, IP and TRCA

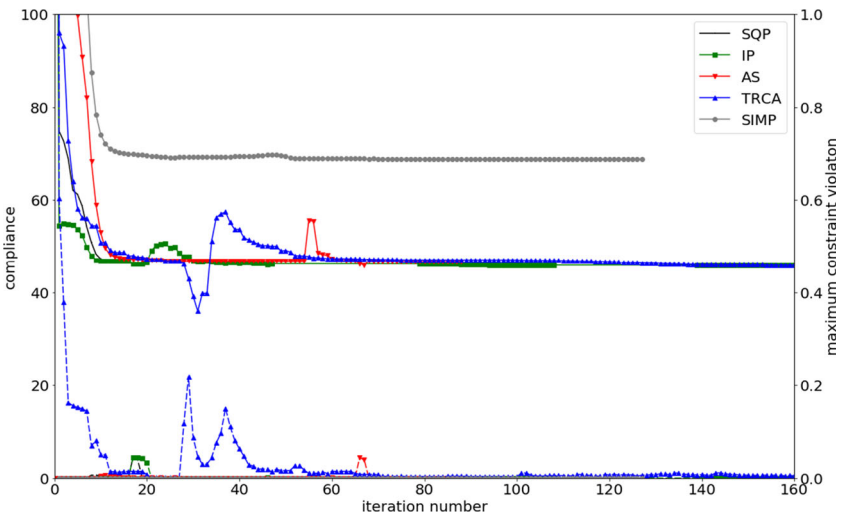

Fig. 9 Compliance evolution and history of constraint violation for short cantilever. The compliance evolution on the left axis is plotted as solid lines, whereas the constraint violation on the right axis is plotted as dashed lines using the same color scheme as the compliance evolution. Total number of function evaluations: SQP: 35, AS: 630, IP: 225, TRCA: 235, SIMP: 127

4.2 Long cantilever structure

The second benchmark problem corresponds to the long cantilever problem studied in Norato et al. (2015). The domain is rectangular with width of twenty and height of five—see Fig. 10. A vertical, downward pointing load of ten is applied at the top right of the domain and two support points are applied at the bottom and top at the left side. The Young modulus is $E = 10^5$ and the Poisson ratio $\nu = 0.3$. Again, the initial layout was a minimal graph containing the two support points and the load. With the larger aspect ratio (width/height = 4), this problem requires more substructure to be developed along the width of the domain. Thus, three cycles were developed for all four mathematical programming algorithms. Figure 11 depicts the initial layout and the optimized solution obtained with SIMP. The SIMP solution was again computed using the code top88.m with the following parameters: number of elements in x and y directions $n_x = 600$, $n_y = 150$, respectively, volume fraction, $v_f = 0.3$, penalization factor, $p = 3$, filter radius, $r_{min} = 6$, filtering of the sensitivities and convergence tolerance of 0.001.

The optimized solutions at the end of the three cycles obtained for each method are shown in Fig. 12. The solutions obtained with the four mathematical programming algorithms agree well with each other for this case, but are markedly different than the optimized solution obtained with SIMP. Again, a direct comparison of compliance obtained with the cellular developmental method and SIMP is not warranted. However, since the layout obtained with the cellular developmental method was noticeably distinct from that obtained with SIMP, we performed a shape optimization starting from SIMP's topology, but with a simpler shape, to optimize the compliance of the frame. The initial and final layouts resulting from this computation are shown in Fig. 13. The layout of the optimized frame agrees well with the layout obtained with SIMP (except for the joints, which in the SIMP solution contain some gray material, and a slight inclination of a lower edge in the frame layout), and its optimized compliance is slightly higher, about 1.4% higher, than the compliance obtained with the cellular developmental method. Therefore, for this problem, the optimized layout obtained by the cellular developmental method performed slightly better than the optimized layout obtained with SIMP in the same context. The proximity of the compliance values suggests once again a flat region around a local minimum.

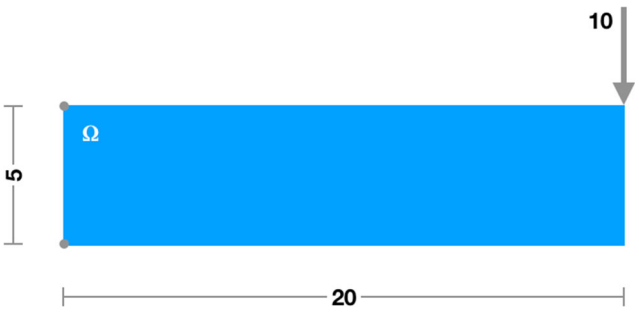

Fig. 10 Design domain for skeleton, external loads and support points (gray disks at left boundary)

Finally, the convergence history of the four mathematical programming algorithms is shown in Fig. 14. Note the slow decrease in the objective function for SIMP and the fact that for this problem the cellular developmental method needs only a fraction of the number of function evaluations of SIMP. The SQP algorithm again performed well, and it is the chosen algorithm for the remaining computations.

4.3 Variations of the theme

The benchmark problems considered thus far demonstrate the aptitude of the cellular developmental method to solve classical problems in topology optimization of structures. The purpose of this subsection is twofold: to explore some features of the cellular developmental method in solving problems that are challenging for conventional methods, and to demonstrate the applicability of the method to problems in complex domains. In this section, all shape optimizations were performed using SQP.

4.3.1 Short cantilever problem with angle constraint

One main advantage of the projection method (Norato et al. 2015) is its ability to handle manufacturing constraints, such as constraints on the thickness of the frame members. Similarly, the cellular developmental method can implement such constraints and controls over the member thicknesses. Another class of essential and challenging manufacturing constraint is the class of constraints on angles associated with the frame members (Garaigordobil et al. 2018). The cellular developmental method provides a natural framework to implement such a class of constraints, and as an illustrative example we consider the constraint on the angles between the members of the frame.

This test case revisits the short cantilever, but now with an added constraint for the minimum angle between the skeleton edges, namely, the angle between incident edges of the skeleton must be greater or equal to 30° for this test case. Compared to the benchmark Section 4.1 (Fig. 8), the layout under the minimum angle constraint (Fig. 15) presented a reduction in the amount of material closer to the right boundary. The receded cross bars lead to the appearance of substructure and an arching of the main bars close to the right boundary. The compliance increased by 3.5% as a result of the added angle constraint.

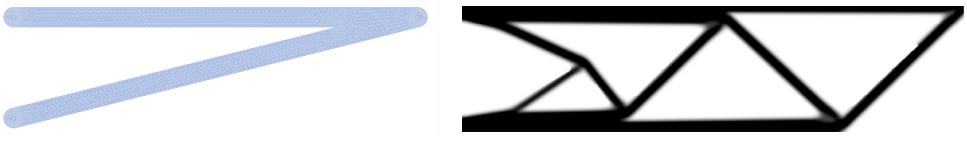

(a) Initial layout (b) SIMP optimized solution

Fig. 11 Long cantilever: (a) initial layout defined as a minimum graph containing the support and load points, (b) optimized solution obtained with SIMP: $\mathcal{J}_c = 0.597$, $A = 30.0$

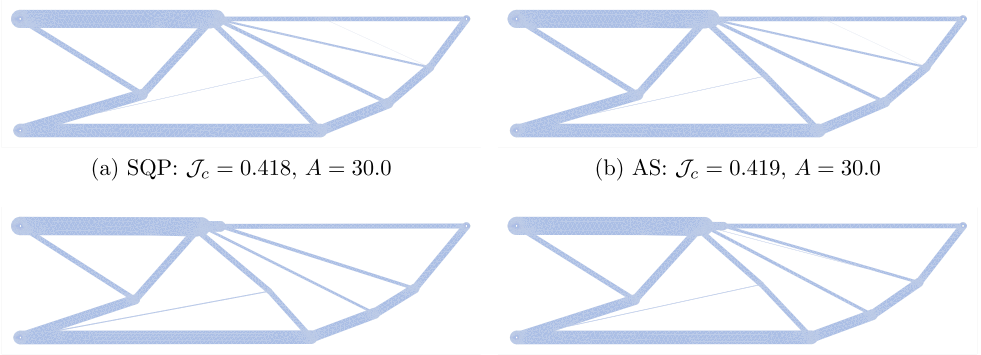

(a) SQP: $\mathcal{J}_c = 0.418$, $A = 30.0$ (b) AS: $\mathcal{J}_c = 0.419$, $A = 30.0$

(c) IP: $\mathcal{J}_c = 0.419$, $A = 30.0$ (d) TRCA: $\mathcal{J}_c = 0.418$, $A = 30.0$

Fig. 12 Long cantilever. Optimized layouts after three cycles obtained with the mathematical programming algorithms SQP, AS, IP and TRCA

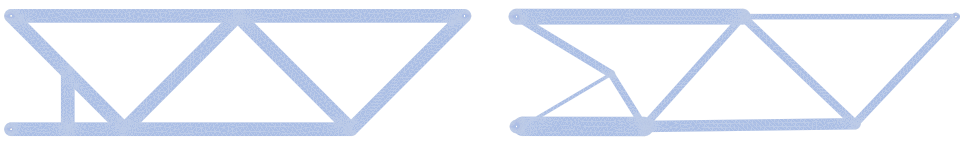

(a) Initial layout (b) Shape optimized solution

Fig. 13 Long cantilever: (a) initial layout defined by SIMP's topology, (b) shape optimized solution obtained with SQP: $\mathcal{J}_c = 0.424$, $A = 30.0$

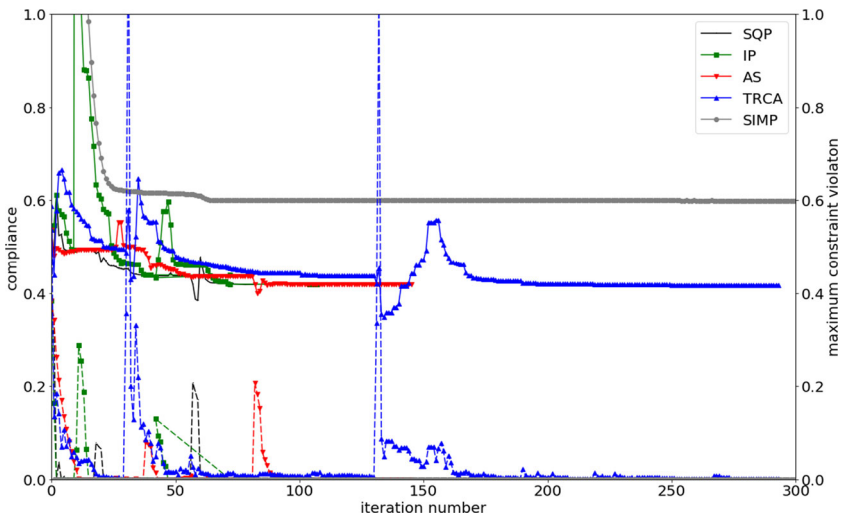

Fig. 14 Compliance evolution and history of constraint violation for long cantilever. The compliance evolution on the left axis is plotted as solid lines, whereas the constraint violation on the right axis is plotted as dashed lines. Total number of function evaluations: SQP: 184, AS: 1189, IP: 165, TRCA: 369, SIMP: 1273

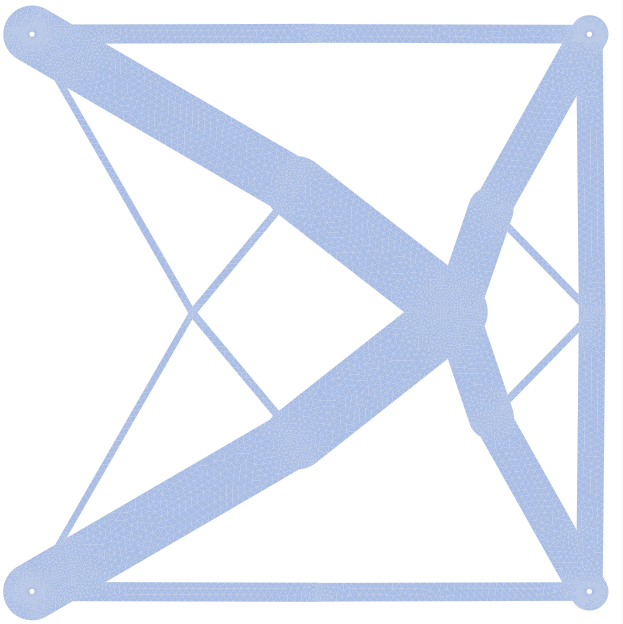

Fig. 15 Frame member parameterization. The geometry of a capped rectangle is defined by five parameters: $\mathcal{J}_c = 47.4$, $A = 0.4$

4.3.2 Unbounded long cantilever problem

Besides the control of thickness and angle between members of the frame, the cellular developmental method can also trivially optimize layout on unbounded domains. In methods such as SIMP, level-set or the projection method, a design domain must be set a priori and the optimization can only be operated inside that design domain. For some problems, the design domain may be unbounded and that poses difficulties to the conventional methods, as such methods would have to adopt a continuation approach to discover the artificially bounded design domain that contains the optimized solution, while concurrently optimizing the layout within each design domain in the continuation process. In the cellular developmental method, the unbounded domain is the natural domain for all optimization problems, and a boxed design domain, such as those considered in the benchmark problems above, requires the addition of bounds on the design variables to fit within the box. In this section, the long cantilever problem was reconsidered, but this time without constraints on the size of the design domain.

In addition, we also explored the two-point topological derivative capability of predicting the change in the compliance of the structure. In Algorithm 1, the division of a cell is performed along the pair minimizing the two-point topological derivative among acceptable pairs on the boundary of a cell. Here additional divisions can be effected along acceptable pairs whose magnitude of the two-point topological derivative is within 25% of the minimizing, acceptable pair.

The result of these modifications is a dramatic change in both the layout and the performance of the optimized solution and the cellular development. Figure 16 shows two cycles of the cellular developmental method. The frame of the cellular developmental method after each cycle resembles the layouts of Michell trusses, and the compliance of the final frame was reduced by 19.5% compared to the compliance to the bounded domain (cf. Figs. 16 and 12). Finally, because of the acceptance of more edges, the final frame was obtained after only two cellular developmental cycles.

4.3.3 L-bracket problem

As mentioned, the design domain in the cellular developmental method is unbounded. In Sections 4.1 and 4.2, the design domain is constrained to box domains. In this section, we present an application of the method to a more complex, non-convex domain, namely, an L-shaped polygonal domain—see Fig. 17.

To implement this domain constraint, we used a signed, forward Hausdorff distance function applied to the edges of the skeleton. Concretely, given an edge, e, of the skeleton and a polygonal domain L, the signed, forward Hausdorff distance function is defined as

$$d(e \to L) = s \max_{p \in e} \min_{q \in L} \|p - q\|, \tag{26}$$

where the sign s is positive if the point, p, in e that maximizes the distance from L lies outside of the domain

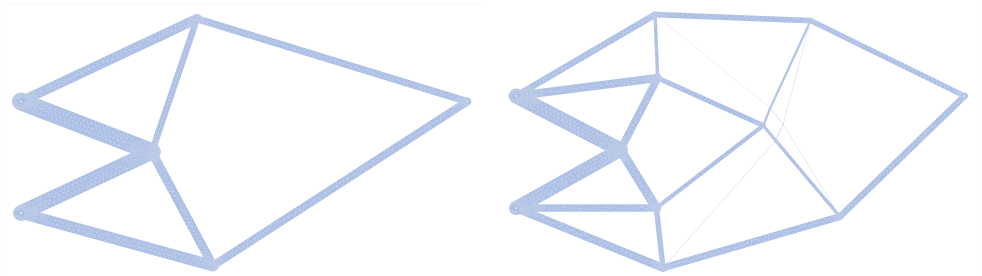

(a) Cycle 1: $\mathcal{J}_c = 0.345$, $A = 30.0$ (b) Cycle 2: $\mathcal{J}_c = 0.324$, $A = 30.0$

Fig. 16 Long cantilever: development cycles of the optimized solution. The initial cycle is the same as in the constrained problem (see Fig. 11a)

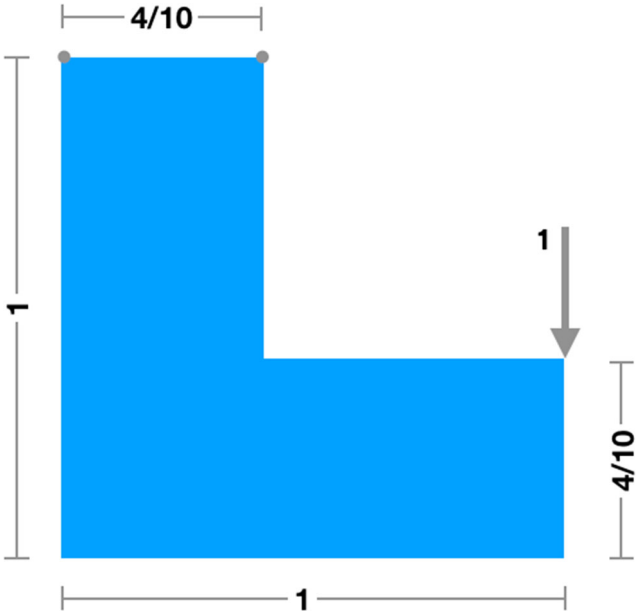

Fig. 17 Design domain for skeleton, external loads and support points (gray disks at top boundary)

L, negative if p lies inside the domain L and zero if p lies on the boundary of L. The initial layout used for this problem was a minimal graph containing the support and load points and an additional barrier edge dividing the non-convex domain L in two convex polygons (Fig. 18a). The point at the re-entrant corner of the domain was kept fixed

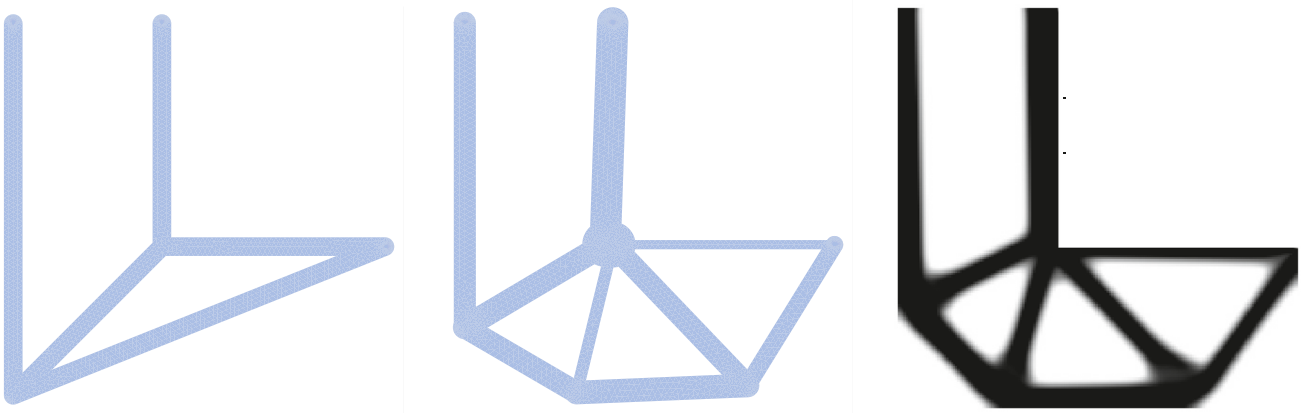

(a) Cycle 0: $\mathcal{J}_c = 397.8$, $A = 0.187$ (b) Cycle 1: $\mathcal{J}_c = 158.7$, $A = 0.256$ (c) Density based TTOM

Fig. 18 L-bracket problem: (a) initial layout depicting the barrier edge splitting the L-bracket into two convex polygons, (b) optimized layout after the first cycle, (c) optimized layout obtained using the thermodynamic topology optimization method (TTOM) reported in Jantos et al. (2019). The figure in (c) is adapted from Jantos et al. (2019)

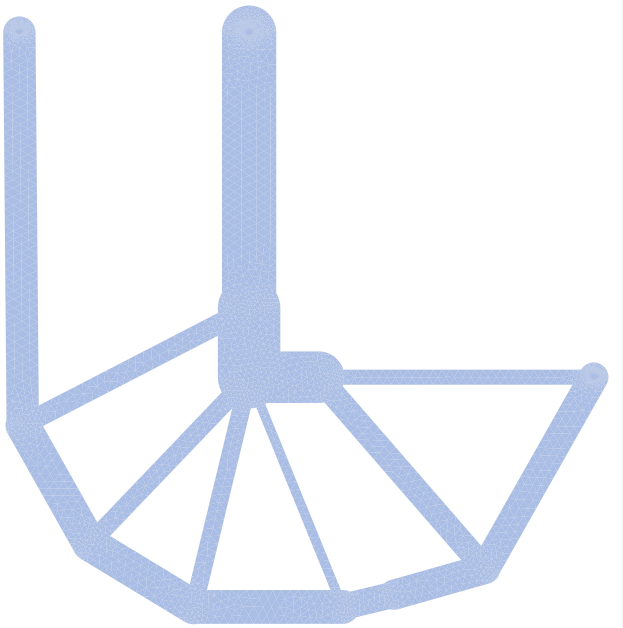

Fig. 19 Optimized layout after cycle 2: $\mathcal{J}_c = 135.5$, $A = 0.256$

during the optimization. The L-bracket is supported at two points at the top of the bracket and a single load is applied at the right tip of the bracket (Jantos et al. 2019) and the target area is 0.256. The optimized layout obtained after the first cycle is shown in Fig. 18b. This layout agrees well with the reference layout obtained using the thermodynamic topology optimization method (TOMM) reported in Jantos et al. (2019). A second cycle is performed using the cellular developmental method resulting in the layout shown in Fig. 19. The final frame introduces novel branches in the optimized frame and results in a reduction of 14.6% in the compliance when compared to the optimized layout after the first cycle.

5 Conclusions

A cellular developmental method for topology optimization of structures was developed via the two-point topological-derivative. The two-point topological derivative entails an additive process, in contrast to the single-point topological derivative that lends itself to a subtractive process. It is expected, therefore, that these two concepts can play complementary roles in the shape-topology optimization of structures. The subtractive method seeks regions of excess material that can be expunged from the layout, whereas the additive method is used to answer two questions: should a new member be added to the frame? If so, which frame members can carry the load more efficiently?

Several optimization problems were considered that demonstrate the aptitude of the method to perform topology optimization of structures. Based on these results, the following conclusions can be drawn.

1. The additive nature of the two-point topological derivative quantifies candidate pathways for load to be transferred within the frame. Because the traditional training of structural engineers relies heavily on the concept of load paths, the novel two-point topological derivative introduced here can provide novel insights into structural design.
2. Methods that are based on basic shapes for modeling the layout of the structure, such as Norato et al. (2015), cannot use single-point topological derivatives, because the basic shapes are not holed (shapes with a predetermined number of holes could be an option in such cases). For the latter methods, the two-point topological derivative is a natural option to avoid local minima determined by connected components of mutually, continuously deforming shapes in the design landscape.
3. Similarly to shape gradients, the two-point topological derivative can be used as a stopping criterion for the cellular division process or serve as a metric for acceptable new edges to be added to the frame.
4. Four mathematical programming algorithms, namely, SQP, AS, IP and TRCA, performed well for the shape optimization. For the problems studied, the SQP provided the overall best performance with respect to both the number of iterations as well as the number of function evaluations needed to meet a pre-defined tolerance.
5. A minimal graph comprising the load and support points sufficed to start the cellular developmental method, with additional members being added as needed and connecting pairs that maximize the decrease in compliance computed with the two-point derivative. If the domain is non-convex, then additional barrier edges that partition the domain into convex subdomains can also be used.
6. The frame protocol adopted in this work is flexible and can be easily modified to parameterize the frame with higher order models. For instance, the shape of each member can be parameterized with Bezier curves supported over the skeleton. This approach would be especially suitable for problems where the stresses at joints in the frame are significant.
7. The mesh in this work was automatically generated for each shape and topology of the frame. We anticipate that the use of an arbitrary Lagrangean-Eulerian approach in conjunction with meshfree methods, such as Lee and Yoon (2004), will speed up the computations.

8. Compared to popular methods, such as SIMP and the level-set method, the cellular developmental method greatly reduces the number of design variables. The latter also allows for easy control over the size of the frame members and the angle between them. In addition, the optimized frame does not need any post-processing and does not require a priori setting of the resolution of the frame features or size of the design domain.
9. Finally, the projection method (Norato et al. 2015) and the cellular developmental method share a number of traits, most notably, the use of primitive shapes to model the layout of the structure. Such choice not only allows for the easy control of the size of the frame's members, but also greatly reduces the number of design variables in the problem. Yet, the cellular division does not need a post processing interpretation of the design, nor an a priori choice of the number of members, and the cellular developmental method can also easily constrain the angle between the members of the topology.

Appendix 1. Two-point topological derivative

Consider the compliance functional (Allaire et al. 2004)

$$\mathcal{J}_c(\Omega) = \int_\Omega Ae(u) : e(u), \tag{27}$$

where $\alpha \geq 2$, $u_\omega \in L^\alpha$ and $k \in L^\infty(D)$ is a non-negative weighting function. Assume $f \in H^1(\Omega)^N$, $g \in H^2(\Omega)^N$ and $u \in H^2(\Omega)^N$. Then, given admissible $p, q \in \partial\Omega$, the two-point topological derivative of the compliance can be written as

$$\begin{aligned}\mathcal{T}\mathcal{J}_c(p,q) = {} & \frac{u_0^\perp(p)+u_0^\perp(q)}{2}\int_0^l f^\perp(x)dx \; + \\ & \frac{u_0^\perp(p)-u_0^\perp(q)}{2l}\int_0^l (l-2x)\, f^\perp(x)dx \; + \\ & \int_0^l \frac{f^\parallel(x)\left\{x\int_0^l\int_0^\eta \frac{f^\parallel(\xi)}{\hat{E}}d\xi d\eta - l\int_0^x\int_0^\eta \frac{f^\parallel(\xi)}{\hat{E}}d\xi d\eta + [(l-x)u(p)+xu(q)].\frac{q-p}{l}\right\}}{l}dx \; - \\ & \frac{(\hat{E})}{2l^2}\int_0^l\left[\frac{(u(p)-u(q)).(q-p)}{l} - l\int_0^x \frac{f^\parallel(\xi)}{(\hat{E})}d\xi + \int_0^l\int_0^\eta \frac{f^\parallel(\xi)}{(\hat{E})}d\xi d\eta\right]^2 dx\end{aligned} \tag{A1.1}$$

where $\hat{E} = E/(1-\nu^2)$ for plane strain, and $\hat{E} = E$ for plane stress or three-dimensional problems, $l = |p-q|$, x is the arc length coordinate along the line $\overline{pq}$ and the superscript $^\parallel$ (resp. $^\perp$) denotes the component parallel (resp. orthogonal) to $\overline{pq}$ oriented from p to q. Indeed, under the hypotheses above, we can use Theorem 7 in Allaire et al. (2004) to obtain

$$\begin{aligned}\mathcal{J}_c'(\Omega_t)(\theta) = {} & \int_{\Gamma_t\cup\Gamma_N}[2 \\ & -Ae(u_t) : e(u_t)]\theta.n \; + \\ & \int_{\Gamma_D}[Ae(u_t) : e(u_t)]\theta.n,\end{aligned} \tag{A1.2}$$

where $\partial_n = \partial/\partial n$, H is the mean curvature of $\partial\Omega$ and $\theta \in W^{1,\infty}(\mathbb{R}^N, \mathbb{R}^N)$. Using the chain rule, it follows that

$$J_c'(t) = \mathcal{J}_c'(\Omega_t)(\partial_t\Omega_t), \tag{A1.3}$$

where $\partial_t\Omega_t$ denotes the geometric sensitivity of the extended domain Ω_t with respect to the parameter t.

We consider first the problem in the plane and let I_t denote a thin ligament connecting points $p, q \in \partial\Omega$. Then using (A1.2) and (A1.3), and the free traction boundary conditions at the ligament boundary, we obtain:

$$J_c'(t) = \int_{\bar{\Gamma}_t}\left(f.u_t - \frac{Ae(u_t) : e(u_t)}{2}\right) = \int_{\bar{\Gamma}_t}\left(f.u_t - \frac{\sigma_{xx}^2}{2\hat{E}}\right), \tag{A1.4}$$

where $\bar{\Gamma}_t$ are the ligament faces that move when changing its thickness. Indeed, $Ae(u_t) : e(u_t) = \sigma_{xx}\epsilon_{xx} + \sigma_{yy}\epsilon_{yy} + 2\sigma_{xy}\epsilon_{xy}$; $\sigma_{yy} = \sigma_{xy} = 0$, on, $\bar{\Gamma}_t$, where y is a coordinate right orthogonal to x and the traction free condition is applied; $\epsilon_{xx} = \frac{1}{\hat{E}}(\sigma_{xx} - \nu\sigma_{yy})$; $\partial_t\Omega_t = n/2$ in $\bar{\Gamma}_t$ and $\partial_t\Omega_t = 0$, otherwise. Therefore, on, $\bar{\Gamma}_t$, where the integration is computed, the equality: $Ae(u_t) : e(u_t) = \frac{\sigma_{xx}^2}{\hat{E}}$ holds as claimed.

Here we present a formal derivation using an approach akin to the derivation of plane stress equations can be employed to approximate the integrand terms—a rigorous (and difficult) approach to the asymptotic expansion of u_t around $t = 0$ for the Poisson problem can be found in Nazarov et al. (2004, 2005). Indeed, taking coordinates (x, y) in the plane with x along the mean line of the

rectangular ligament, the equilibrium equation can be written as follows:

$$\partial_x \sigma_{xx} + \partial_y \sigma_{yy} + f = 0. \tag{A1.5}$$

Integrating over y, using the traction-free boundary at $y = \pm t/2$ and using the averages over the thickness $\bar{\sigma}_{xx} = 1/t \int_{-t/2}^{t/2} \sigma_{xx}$, $\bar{f} = 1/t \int_{-t/2}^{t/2} f$, we obtain:

$$\partial_x \bar{\sigma}_{xx} + \bar{f} = 0. \tag{A1.6}$$

Finally, using the constitutive law

$$\epsilon_{xx} = \frac{1}{\hat{E}}(\sigma_{xx} - \nu \sigma_{yy}), \tag{A1.7}$$

the kinematic relation

$$\epsilon_{xx} = \partial_x u, \tag{A1.8}$$

and averaging over the thickness results in

$$\hat{E}(\bar{u}_d)'' + f^{\parallel} = 0, \tag{A1.9}$$

within the domain, while at the boundaries

$$\bar{u}_d(0) = u_0^{\parallel}(p), \tag{A1.10}$$

$$\bar{u}_d(l) = u_0^{\parallel}(q). \tag{A1.11}$$

Here the average displacement in the ligament has been decomposed as

$$\bar{u}_t = (\bar{u}_t + \bar{u}_r)e_{\perp} + \bar{u}_d e_{\parallel}, \tag{A1.12}$$

where $\bar{u}_t$ represents the translation of the centroid of the line $\overline{pq}$ by a displacement equal to arithmetic mean of the components normal to the line $\overline{pq}$ at the ends p and q, $\bar{u}_r$ is a rotation component around the centroid of the line $\overline{pq}$ and $\bar{u}_d$ the mean deformation along the ligament around $\overline{pq}$. Symbolically,

$$\bar{u}_t(x) = \frac{u_0^{\perp}(p) + u_0^{\perp}(q)}{2}, \tag{A1.13}$$

$$\bar{u}_r(x) = \frac{u_0^{\perp}(p) - u_0^{\perp}(q)}{2l}(l - 2x), \tag{A1.14}$$

where x is the arc length coordinate along the line $\overline{pq}$ with origin at p and l is the length of the line $\overline{pq}$. Therefore,

$$\bar{u}_d(x) = u_0^{\parallel}(p) - \frac{u_0^{\parallel}(q) + u_0^{\parallel}(p)}{l}x - \frac{x}{l}\int_0^l \int_0^{\eta} \frac{f^{\parallel}(\xi)}{2\mu + \hat{\lambda}} d\xi d\eta + \int_0^x \int_0^{\eta} \frac{f^{\parallel}(\xi)}{2\mu + \hat{\lambda}} d\xi d\eta. \tag{A1.15}$$

Replacing (A1.13), (A1.14) and (A1.15) into (A1.12) and the latter into (A1.4) and taking the limit as $t \to 0$ yields (A1.1) (after simplification and noting that the rigid motions $\bar{u}_t$ and $\bar{u}_r$ do not create strain). The case of three-dimensions is obtained analogously.

If the body forces are negligible, then

$$\mathcal{TJ}_c(p, q) = -\frac{\hat{E}}{|q - p|^3}[(u(q) - u(p)).(q - p)]^2. \tag{A1.16}$$

We note in passing that in the absence of significant body forces, the addition of a bar in a frame will never increase the compliance of the frame, while increasing the mass of the frame; and also the resemblance of (A1.9) to the equilibrium equation on a truss member. The latter agrees with the fact that truss equations are obtained from the continuum equations under the assumption of thin members.

Appendix 2. Finite differences verification

To verify the correctness of the numerical implementation of the topological derivative, a comparison was carried-out between the results computed with the analytical topological derivative in (14) against the following one sided finite difference approximation:

$$\mathcal{T}_{FD}\mathcal{J}(p, q; t) = \frac{\mathcal{J}(\Omega + I_t) - \mathcal{J}(\Omega)}{t}. \tag{A2.1}$$

The problem selected for the verification is the test case Section 4.2, with the points selected for probing given by:

$$p = (5.75, 4.625), \tag{A2.2}$$

$$q = (9.484611796797793, 2.7576941016011034). \tag{A2.3}$$

These points correspond to boundary points along the line connecting an approximation to the minimum pair for the compliance derivative.

Figure 20 shows the error of the finite-difference approximation as a function of the thickness of the ligament. A

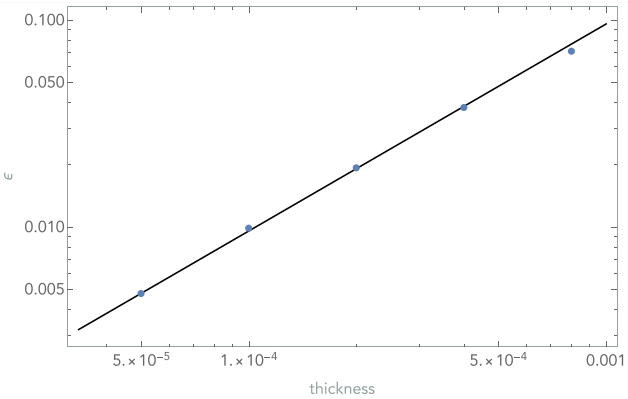

Fig. 20 Single-load-case cantilever. Logarithmic plot of the absolute error in the finite-difference approximation of the two-point topological derivative as a function of the thickness of the ligament. Dots: finite-difference error. Solid-line: degree one slope. Lagrangian $\mathbb{P}_3$ finite-elements are used in the analyses with adaptive mesh refinement with compliance as target functional. The number of degrees-of-freedom in each computation varies from 893,046 for the thickness equal to 5×10^{-5}, to 1,214,328 for the thickness equal to 8×10^{-4}

Table 1 Comparison of estimated compliance and actual compliance. Compliance at Ω_0: $\mathcal{J}_c = 0.7321131267730081$

Thickness	$\mathcal{J}_c(\Omega_t)$	$\mathcal{J}_c(\Omega_0) + \mathcal{T}\mathcal{J}_c(\Omega_0) \times$ thickness	δ [%]
8×10^{-4}	0.7316465312091498	0.7315895678974905	89.12
4×10^{-4}	0.7318664308138638	0.7318513473352494	94.2381
2×10^{-4}	0.731986114928322	0.7319822370541287	97.0373
1×10^{-4}	0.7320486713150742	0.7320476819135684	98.4882
5×10^{-5}	0.7320806442001073	0.7320804043432882	99.267

Two point topological derivative at Ω_0: $\mathcal{T}\mathcal{J}_c = -0.654448594397$. Accuracy of estimate $\delta = |\mathcal{T}\mathcal{J}_c(\Omega_0) \times \text{thickness}/[\mathcal{J}_c(\Omega_t) - \mathcal{J}_c(\Omega_0)]|$

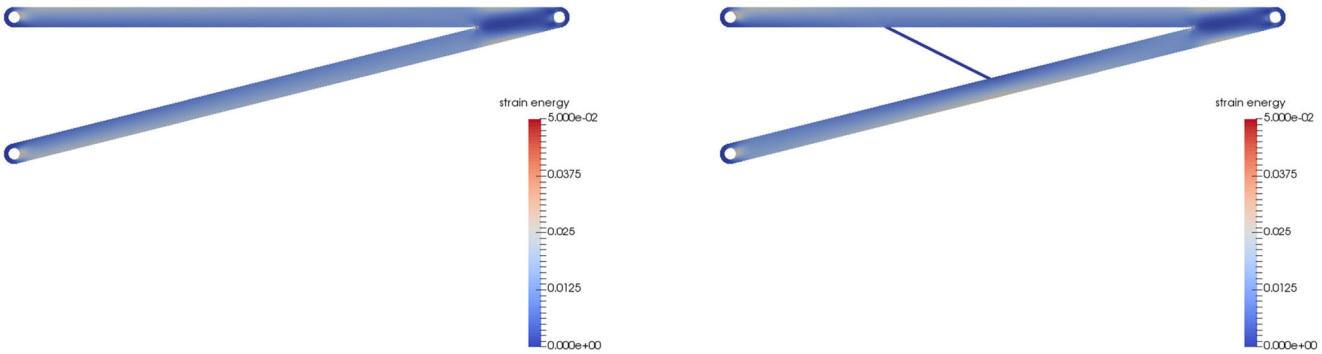

(a) Initial layout: $v_f = 0.295886, \mathcal{J}_c = 0.732113$ (b) Deformed layout: $v_f = 0.300052, \mathcal{J}_c = 0.727937$

Fig. 21 Single-load-case cantilever. Distribution of strain-energy in the initial and deformed layouts. Isthmus thickness: 0.1. Lagrangian $\mathbb{P}_3$ finite-elements are used in the analyses with adaptive mesh refinement with compliance as target functional

linear decay of the error for the one-sided finite-difference approximation is observed, which verifies the correctness of the implementation. As shown in Table 1, the two-point topological derivative can also be used to estimate the reduction of the compliance by the addition of the quadrilateral bar with varying thicknesses. As expected, the accuracy of the estimate improves with as the bar becomes thinner, but it is still accurate for the thickest bar listed. Finally, Fig. 21 shows the distribution of strain energy on the initial layout, and the topology of the deformed initial layout with an ligament at the sample pair p, q. This figure shows that connecting the two points along their connecting line reduces the compliance around those points enough to decrease the compliance of the overall frame, despite the additional strain energy generated in the new, connecting bar.

Funding During the performance of this work, the first author has been partially funded by the contract RSC19041 with the University of Dayton Research Institute, under the AFRL CRDinAL project.

Declarations

Conflict of interest The authors declare that they have no conflict of interest.

Replication of results The implementation of the methodology above was carried-out using open-source software with appropriate citation in the text. The values of the parameters used to obtain the results as well as the outcome values of the compliance and area were also provide, both of which can be used for replicating and verifying the results.

References

Allaire G, Jouve F, Toader A-M (2004) Structural optimization using sensitivity analysis and a level-set method. J Comput Phys 194:363–393

Alnaes MS, Blechta J, Hake J, Johansson A, Kehlet B, Logg A, Richardson C, Roing J, Rognes ME, Wells GN (2015) The FEniCS project version 1.5. Archive of Numerical Software 3

Andreassen E, Clausen A, Schevenels M, Lazarov BS, Sigmund O (2011) Efficient topology optimizatioin in matlab using 88 lines of code. Struct Multidiscip Optim 43:1–16

Bendsøe MP, Sigmund O (2003) Topology optimization: theory, methods and applications, 2nd edn. Springer, Berlin

Bielefeldt BR, Reich GW, Beran PS, Hartl DJ (2019) Development and validation of a genetic l-system programming framework for topology optimization of multifunctional structures. Comput Struct 218:152–169

Canfield RA (2020) slp_sqp https://www.mathworks.com/matlabcentral/fileexchange/53331-slp_sqp

Dapogny C (2020) A connection between topological ligaments in shape optimization and thin tubular inhomogeneities. Compt Rend Math 358:119–127

Dapogny C (2021) The topological ligament in shape optimization: a connection with thin tubular inhomogeneities hal-02924929

de Berg M, Cheong O, van Kerveld M, Overmars M (2010) Computational Geommetry—Algorithms and applications, 3rd edn. Springer, Berlin

Deaton JD, Grandhi RV (2014) A survey of structural and multidisciplinary continuum topology optimization: Post 2000. J Struct Multidiscip Optim 49:1–38

Eschenauer H, Kobelev V, Schumacher A (1994) Bubble method for topology and shape optimization of structures. Struct Optim 8:42–51

Gangl P (2020) A multi-material topology optimization algorithm based on the topological derivative, computer methods. Appl Mech Eng 366:113090

Garaigordobil A, Ansola R, Santamaría J, de Bustos IF (2018) A new overhang constraint for topology optimization of self-supporting structures in additive manufacturing. Struct Multidiscip Optim 58:2003–2017

Geuzaine C, Remacie J-F (2009) Gmsh: a three-dimensoianal finite element mesh generator with built-in pre- and post-processing facilities. Int J Numer Methods Eng 79:1309–1331

Jantos DR, Hackl K, Junker P (2019) An accurate and fast regularization approach to thermodynamic topology optimization. Int J Numer Methods Eng 117:991–1017

Kobayashi MH, Pedro H-T, Kolonay RM, Reich GW (2009) On the cellular division method for aircraft structural design. Aeronaut J 113:821–831

Lee S-H, Yoon Y-C (2004) Meshfree point collocation method for elasticity and crack problems. Int J Numer Methods Eng 61:22–48

Lee S-H (2008) Removing holes in topological shape optimization. ESAIM: Control Optim Calc Var 14:160–191

Leugering G, Sokolowski J (2008) Topological sensitivity analysis for elliptic problems on graphs. Control Cybern 37:971–997

MathWorks fmincon (2020) https://www.mathworks.com/help/optim/ug/fmincon.html

Michell GM (1904) The limits of economy of material in frame structures. Phil Mag 47:589–597

Nazarov S, Slutskij A, Sokolowski J (2005) Topological derivative of the energy functional due to formation of a thin ligament on a spatial body. Folia Math 12:39–72

Nazarov SA, Sokolowski J (2004) The topological derivative of the dirichlet integral under formation of a thin ligament. Sib Math J 45:341–355

Norato JA, Bell BK, Tortorelli DA (2015) A geometry projection method for continuum-based topology optimization with discrete elements. Comput Methods Appl Mech Eng 293:306–327

Novotny A, Sokolowski J (2020) An introduction to the topological derivative method. Springer Nature, Switzerland

Novotny AA, Sokołowski J, Zochowski A (2019a) Topological derivatives of shape functionals. Part I: Theory in singularly perturbed geometrical domains. J Optim Theory Appl 180:341–373

Novotny AA (2019b) 6Pt width Topological derivatives of shape functionals. Part II: First-order method and applications. J Optim Theory Appl 180:683–710

Novotny AA (2019c) 6Pt width Topological derivatives of shape functionals. Part III: Second-order method and applications. J Optim Theory Appl 181:1–22

Prusienkiewicz P, Lindenmayer A (2004) The algorithmic beauty of plants. Springer, New York

Schittkowski K (1983) On the convergence of a sequential quadratic programming method with an augmented lagrangian line search function. Math Oper Stat Ser Optim 14:197–216. Details of NLPQL

Schmit LA (1960) Structural design by systematic synthesis. In: Proceedings of the second ASCE conference on electronic computation. New York, pp 105–122

Smith HA, Norato JA (2019) A geometry projection method for the design exploration of wing-box structures. In: Proceedings of the SciTech Forum. AIAA, San Diego

Sokolowski J, Zochowski A (1999) On the topological derivative in shape optimization. SIAM J Control Optim 37:1251–1272

Virtanen P, Gommers R, Oliphant TE, Haberland M, Reddy T, Cournapeau D, Burovski E, Peterson P, Weckesser W, Bright J, van der Walt SJ, Brett M, Wilson J, Jarrod Millman K, Mayorov N, Nelson ARJ, Jones E, Kern R, Larson E, Carey C, Polat İ, Feng Y, Moore EW, Vand erPlas J, Laxalde D, Perktold J, Cimrman R, Henriksen I, Quintero EA, Harris CR, Archibald AM, Ribeiro AH, Pedregosa F, van Mulbregt P (2020) SciPy 1.0: Fundamental Algorithms for Scientific Computing in Python. Nat Methods 17:261–272